Article

Biomechanical Analysis of Allograft Spacer Failure as a Function of Cortical-Cancellous Ratio in Anterior Cervical Discectomy/Fusion: Allograft Spacer Alone Model

Ji-Won Kwon [1,2], Hwan-Mo Lee [1], Tae-Hyun Park [3], Sung Jae Lee [3], Young-Woo Kwon [3], Seong-Hwan Moon [1] and Byung Ho Lee [1,*]

[1] Department of Orthopedic Surgery, Yonsei University College of Medicine, Seoul 03722, Korea; kwonjjanng@nhimc.or.kr (J.-W.K.); HWANLEE@yuhs.ac (H.-M.L.); SHMOON@yuhs.ac (S.-H.M.)

[2] Department of Orthopedic Surgery, National Health Insurance Service Ilsan Hospital, Goyang 410719, Korea

[3] Department of Biomedical Engineering, College of Biomedical Science & Engineering, Inje University, Gyeongnam 621749, Korea; thyun06@gmail.com (T.-H.P.); sjl@bme.inje.ac.kr (S.J.L.); voicians0908@gmail.com (Y.-W.K.)

* Correspondence: bhlee96@yuhs.ac; Tel.: +82-2-2228-2180

check for updates

Abstract: The design and ratio of the cortico-cancellous composition of allograft spacers are associated with graft-related problems, including subsidence and allograft spacer failure. Methods: The study analyzed stress distribution and risk of subsidence according to three types (cortical only, cortical cancellous, cortical lateral walls with a cancellous center bone) and three lengths (11, 12, 14 mm) of allograft spacers under the condition of hybrid motion control, including flexion, extension, axial rotation, and lateral bending,. A detailed finite element model of a previously validated, three-dimensional, intact C3–7 segment, with C5–6 segmental fusion using allograft spacers without fixation, was used in the present study. Findings: Among the three types of cervical allograft spacers evaluated, cortical lateral walls with a cancellous center bone exhibited the highest stress on the cortical bone of spacers, as well as the endplate around the posterior margin of the spacers. The likelihood of allograft spacer failure was highest for 14 mm spacers composed of cortical lateral walls with a cancellous center bone upon flexion (PVMS, 270.0 MPa; 250.2%) and extension (PVMS: 371.40 MPa, 344.2%). The likelihood of allograft spacer subsidence was also highest for the same spacers upon flexion (PVMS, 4.58 MPa; 28.1%) and extension (PVMS: 12.71 MPa, 78.0%). Conclusion: Cervical spacers with a smaller cortical component and of longer length can be risk factors for allograft spacer failure and subsidence, especially in flexion and extension. However, further study of additional fixation methods, such as anterior plates/screws and posterior screws, in an actual clinical setting is necessary.

Keywords: cervical spine surgery; allograft spacer; subsidence; finite element model

1. Introduction

The incidence of degenerative cervical spine diseases (DCSD) was varied from 1684 to 1767 per 100,000 population stratified according to disease codes in the Republic of Korea from 2012 to 2016 [1]. In the USA, the incidence of surgery for DCSD rose by almost 150% over the last three decades and stabilized at slightly over 70 operations/100,000 people [2]. The mean age at surgery was 53.3 years, and women underwent 44.4% of all cervical spine surgeries [2]. Anterior cervical discectomy and fusion (ACDF) is a standard treatment for DCSD [3,4]. Instead of using tricortical autologous bone

grafts and titanium polyetheretherketone cages [3,5–8], cervical allograft spacers have been commonly utilized because of their absence of donor site morbidity and physical properties that are similar to those of the natural vertebral body [3,9–11]. A few studies have examined the biomechanical stability of allografts compared with autografts using cadaveric cervical spines; [10]. however, no study has examined allograft spacers and the risk of subsidence on endplates.

From a biomechanical point of view, the design and ratio of cortico-cancellous composition of allograft spacers have been shown to be associated with graft-related problems, including subsidence and allograft spacer failure, leading to breakage and dislodging in clinical settings [12,13]. The present study used finite element model (FEM) analysis to investigate the associations of different cortico-cancellous ratios of cervical allograft spacers with physical stress on the spacers and with subsidence risk on the endplate and vertebral body in involved spinal segments. All experiments were conducted under the condition of hybrid motion control, including flexion, extension, axial rotation, and lateral bending.

2. Materials and Methods

2.1. FEM of an Intact Cervical Spine

A previously validated, three-dimensional, intact model of a C3–7 segment from a 54-year-old male was used for the present study [14,15]. The geometrical data of the multi-segmental cervical model were reconstructed from computed tomography (CT) images. Axial CT scans were obtained with a slice thickness of 0.5 mm and a pixel width of 0.429 mm.

The material properties were selected from the published literature (Table 1). The detailed FEM included vertebral bodies, bony posterior elements, intervertebral discs, and six major groups of ligaments: anterior longitudinal, posterior longitudinal, ligament flavum, facet capsular, interspinous, and supraspinous. The origins and insertions of these ligaments were obtained from a morphological study. The spinal ligaments adopted the nonlinear load-displacement property for the physiological nonlinear behavior of the ligaments [14,16]. The vertebral body consisted of an outer shell of high strength cortical bone reinforced internally by cancellous bone and had an average thickness of 0.5 mm in both cancellous bone and endplates [17]. 3D hexahedral element (eight-node brick) were used as vertebral body-disc structures and posterior element of which material properties were assumed to be homogeneous and isotropic [18–21]. However, the structures of interface between implant and vertebral body were remeshed to 3D tetrahedron (four-node brick) for element refining at interest site. The region of interest between implants and the bone-implant interface was set up using different element sizes that could be distinguished from other parts (implant and periphery, element size = 0.5 mm; the others, 2 mm). Region of interest between implants and the bone-implant interface were set up using different element sizes that could be distinguished from other parts (implant and periphery, element size = 0.5 mm; the others, 2 mm) The mesh convergence in the present study was decided among varying element sizes ranging from 0.5 to 2.0 mm. With an element size of 0.5 mm, the peri-implant converged properly. Finally, a 0.5 mm element size was applied in our surgical model for the translation of experimental results. No unusual stress patterns were observed in this study for this setting.

The intervertebral disc was modeled as a fiber-reinforced structure surrounding the incompressible inviscid nucleus pulposus. The reinforcement structure annulus fibers were modeled by truss elements with modified tension-only properties, with an orientation of about 25° [19,22]. The facet joint was oriented at 45° from the horizontal plane, where the initial surface gaps between each facet region was assumed to be 0.5 mm based upon CT imaging. The facet joint was oriented at 45° from the horizontal plane, where initial surface gaps between each facet region are assumed to be 0.5 mm based upon CT imaging. The interaction of facet joints worked toward increasing the contact force with the narrowing initial gap distance between the upper and lower facet surfaces [22]. The segmental angular measures used to create the lordotic curve for the model were as follows: C3–4, 4.35°; C4–5, 1.87°; and C5–6,

3.94° [23]. For this study, the general-purpose FEA package ABAQUS (Abaqus 2017, Dassault Systèmes Simulia Corp., Providence, RI, USA.)- the non-linear geometry parameter (NLGEON=ON) in ABAQUS step module was used.

Table 1. Peak stress levels of motion in the motion model.

Component Name	Young's Modulus (MPa)	Poisson's Ratio	Ref.
Cortical bone	12,000	0.3	[22]
Cancellous bone	100	0.29	[18]
Posterior element	3.500	0.29	[16]
End plate	500	0.4	[19]
Annulus matrix	4.2	0.45	[19]
Annulus Fibers	500	Cross-sectional Area 0.1 (mm^2)	[20]
Nucleus pulposus	1.0	0.499 (Incompressible)	[19]

2.2. Allograft Spacer Model

The geometries of a cortical cervical spacer (cortical only: CO; DCI Donor Services Tissue Bank, Nashville, TN, USA), a cortical cancellous cervical spacer (cortical cancellous: CC; DCI Donor Services), and a Cornerstone[TM] ASR (cortical lateral walls with a cancellous center bone: CLC; Medtronic Sofamor Danek, Memphis, TN, USA) were constructed based on measuring the allograft spacer using SolidWorks CAD drawings (Solidworks 2013, Dassault systemes Solidworks Corporation, Waltham, MA, USA) (Figure 1, Table 2) and imported into Abaqus (Abaqus 2017, Dassault Systèmes Simulia Corp., Providence, RI, USA) for meshing. The size of three different allograft spacers was meshed 0.5 mm. And then, the interface behavior, such as CC and CLC, between cortical bone and cancellous bone of the allograft spacer was accomplished through a "tie" contact condition.
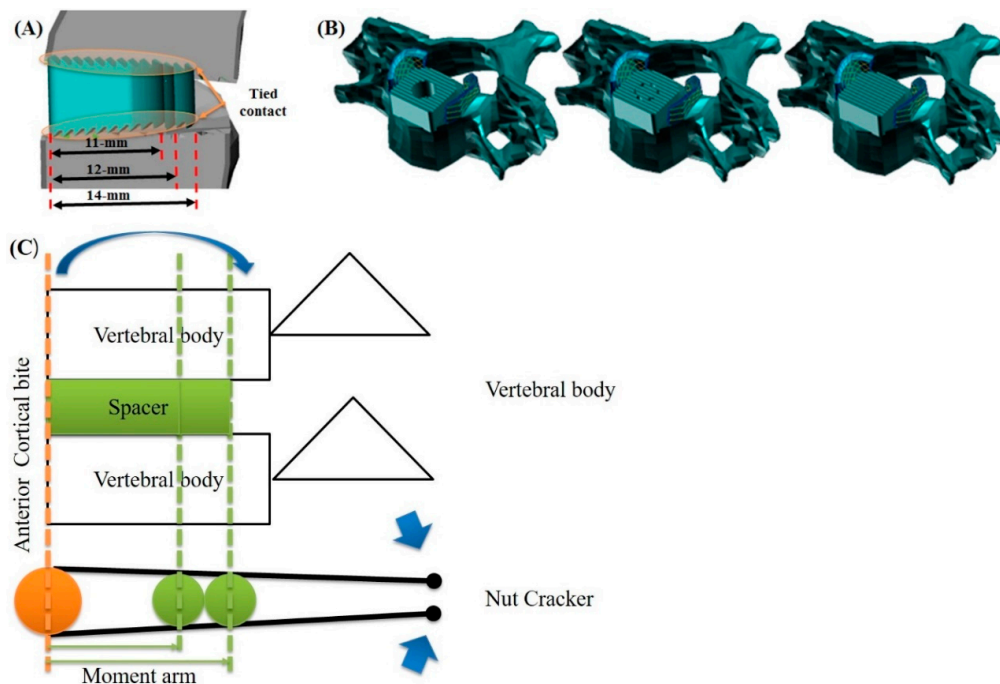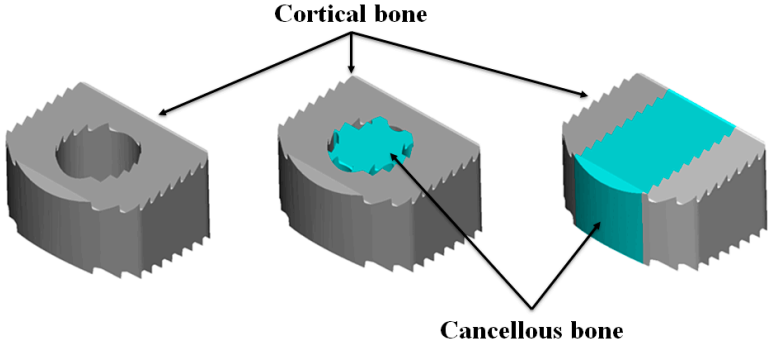

Figure 1. Design of allograft spacers. Length and position of allograft spacers. (**A**) Anterior cortical bite positioning of allograft spacers (**B**) Types of allograft spacers: CO, cortical only; CC, cortico-cancellous; CLC, cortical lateral walls with a cancellous center bone, in that order. (**C**) Schema of the nutcracker mechanism upon flexion and extension in anterior cortical bite positioning of allograft spacers.

Table 2. Cortical-cancellous bone ratio of allospacers.

Cortical bone

Cancellous bone

	Cortical only		Cortico-Cancellous		Cortical lateral Walls with a Cancellous Center Bone	
	Cortical	Cancellous	Cortical	Cancellous	Cortical	Cancellous
11 mm	1	0	1	0.32	0.46	0.54
12 mm	1	0	1	0.28	0.47	0.53
14 mm	1	0	1	0.23	0.47	0.53

Then, each meshed spacer model was inserted into the C5–6 disc without plate fixation in the previously constructed, intact cervical FEM. The spacers used for modeling were 11, 12, or 14 mm in length, had 6° of lordotic angle, and were 7 mm in height, which best fit the vertebral anatomy at the C5–6 level of the cervical model used in this study. The material properties of the allograft spacers (cortical bone, elastic modulus (E) = 18,200 MPa, Poisson's ratio (v) = 0.38; cancellous bone, E = 389 MPa, (v) = 0.3) were measured on a donor femur according to previous research [24,25]. The devices were designed to be implanted via an anterior surgical approach, as recommended by the manufacturer. By simulating this surgical procedure [26], the anterior longitudinal ligament, the superior and inferior endplates, and the anterior and posterior parts of the annulus fibrosus were excised. Then, the spacers were positioned at the anterior margin of the vertebral body (Figures 1 and 2). Because our model aimed to simulate biomechanical behavior after bony fusion, specific corresponding constraint conditions were set up, especially at the bone-implant interface. In this study, interface behavior was accomplished through a "tie" contact condition, which enabled the allograft spacer and vertebrae to be bonded together permanently with full constraint.
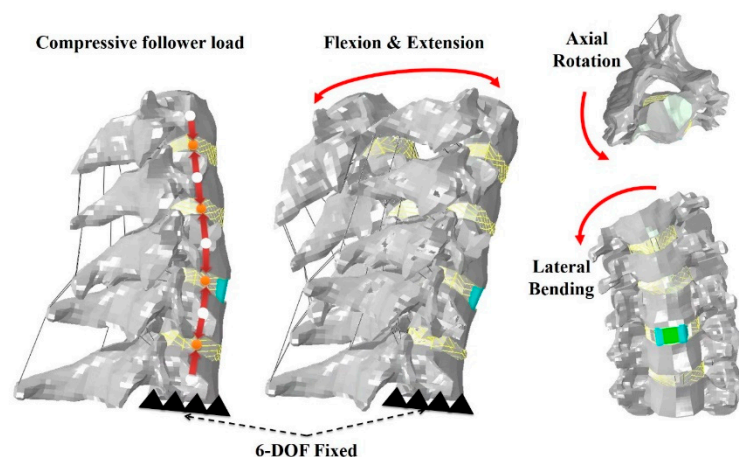

Figure 2. Finite element model of allograft spacers with hybrid motion control.

2.3. Loading and Boundary Conditions

The inferior endplate of the most caudal vertebra (C7) was fixed in all degrees of freedom, while loads were applied to the superior endplate of the most cephalic vertebral vertebra (C3).

The follower load allows each individual vertebra to be loaded in nearly pure compression. In the present FEM, the intervertebral body was connected at approximately the center of rotation of vertebral bodies C3 through C7 [27]. In loading control, pure moments of 1.0 Nm were generated by a force coupled to flexion, extension, lateral bending, or axial rotation of the cervical spine.

A compressive follower load of 73.6 N was considered to approximate the head weight and local muscle stabilization during daily activity (Figure 2) [14]. A hybrid protocol was used to predict range of motion (ROM) at the surgical site and adjacent levels [28].

3. Results

3.1. Range of Motion

The validated ROM of our intact FEM model was within the acceptable range, compared with cadaver studies [29,30] Upon flexion, the ROM at C4–5 was increased in all spacer models, compared with that in the intact model. The ROM of C5–6 (fused segment) was significantly decreased in all spacer models (Figure 3). Upon extension, when compared with the intact model, the ROM at the C4–5 and C6–7 segments was increased in all spacer models. The ROM of C5–6 was significan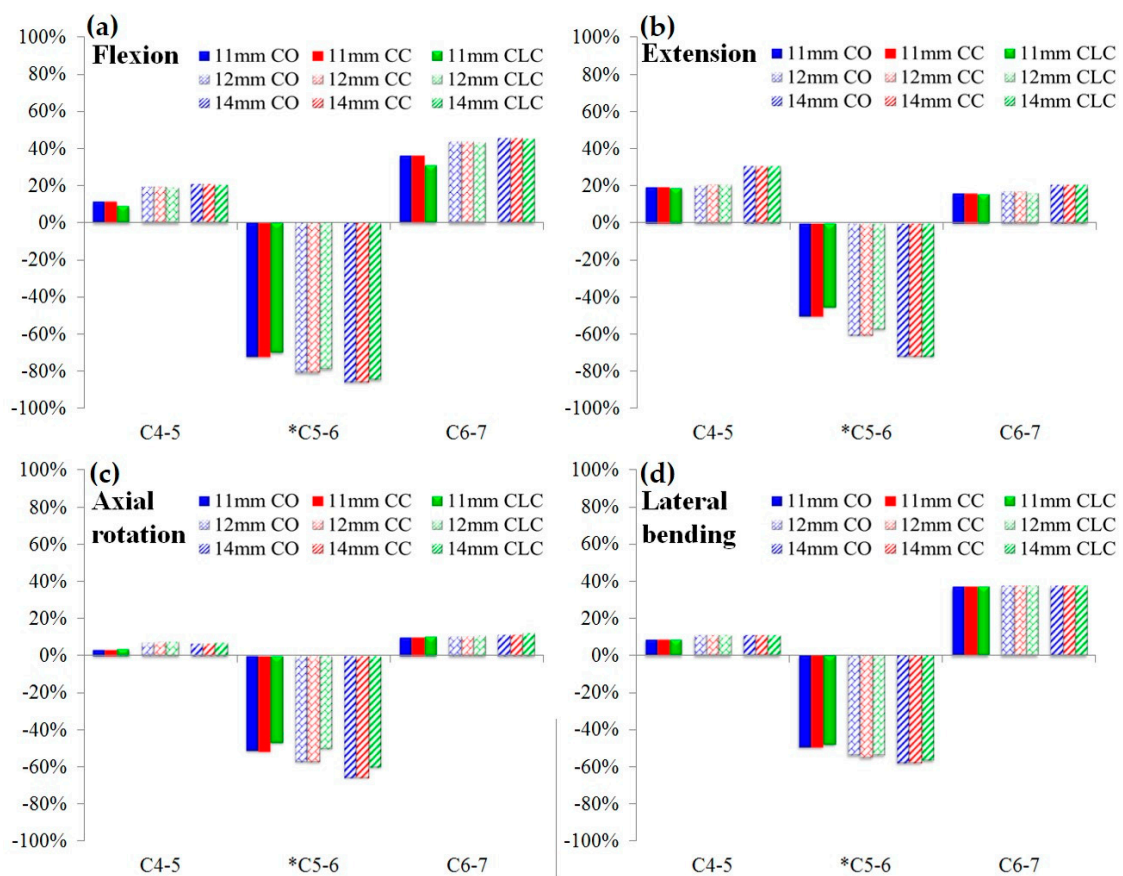tly decreased in all spacer models. In axial rotation and lateral bending, when compared with the intact model, the ROM at the C4–5 and C6–7 segments was increased in all spacer models. The ROM of C5–6 was significantly decreased in all spacer models.

Figure 3. Effects of different cervical allograft spacers on the range of motion, compared with that in an intact model: (**a**) flexion (**b**) extension (**c**) axial rotation (**d**) lateral bending. * indicates fused cervical segment with allograft spacers. CO, cortical only; CC, cortico-cancellous; CLC, cortical lateral walls with a cancellous center bone.

3.2. Stress Analysis of Cervical Spacers with Different Cortico-Cancellous Ratios

In flexion and extension, von Mises stress increased as the length of spacers increased for all types of allograft spacers. The CLC spacer demonstrated the highest stress among the three types of spacers. In counterclockwise axial rotation, von Mises stress decreased as the lengths of spacers increased. In right lateral bending, von Mises stress decreased as the lengths of the CO and CC spacers increased. However, among CLC spacers, PVMS increased as the length of the spacer increased. Stress on the anterior cortical portion increased as the length of spacers increased. The CLC spacers demonstrated the highest stress on the anterior cortical portion among the three types of spacers in the study. (Figure 4). The likelihood of allograft spacer failure was calculated on the basis of the yield strength of the femoral cortical bone (107.9 MPa). The allograft failure risk was calculated using the following formula [31]:

$$\text{Failure risk} = \frac{Stress\ on\ the\ cortial\ portion\ of\ allograft\ spacer}{Yield\ strength\ of\ Femoral\ cortical\ bone\ (107.9MPa)} \times 100. \tag{1}$$
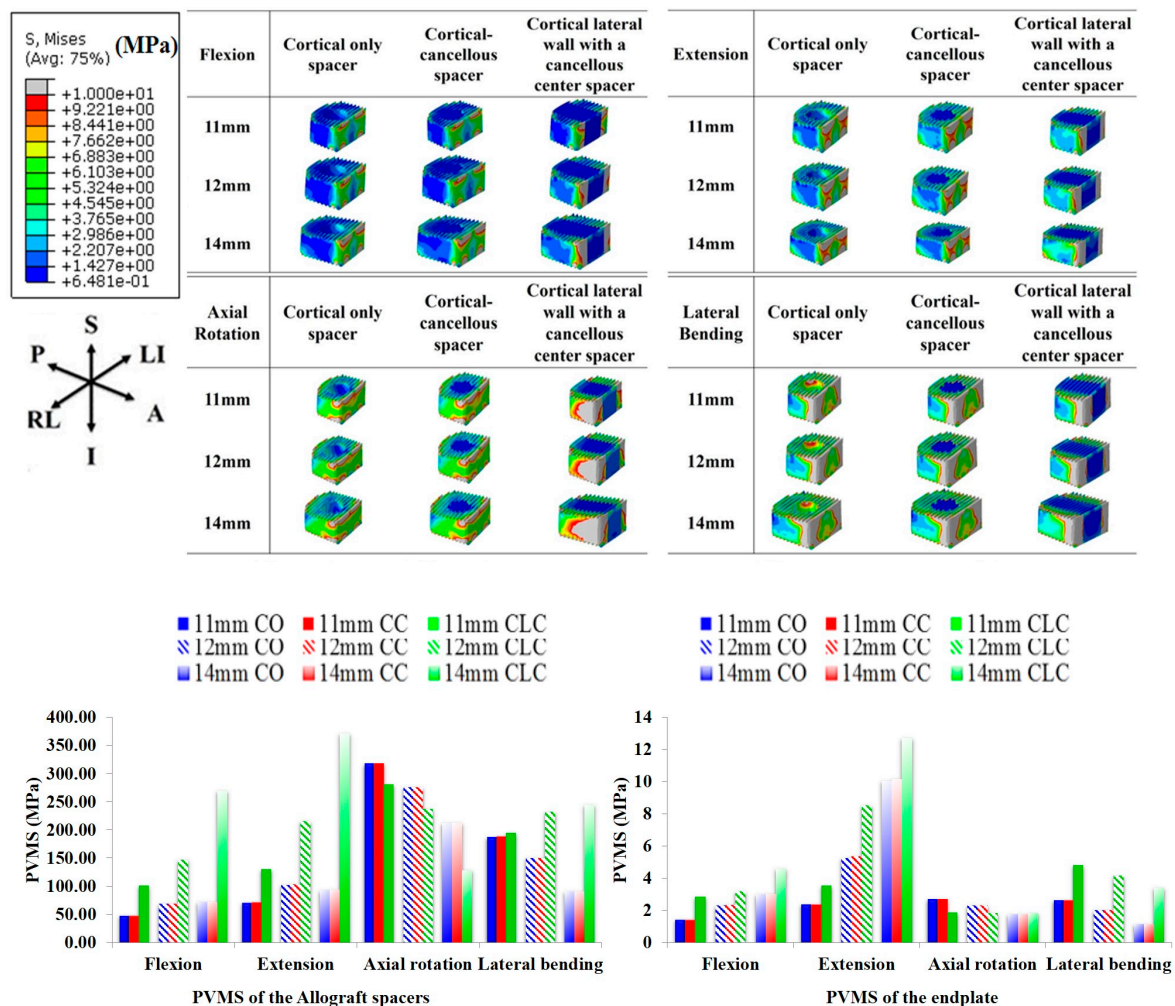

Figure 4. Peak von Mises stress (PVMS) on the allograft spacers and endplates under hybrid motion.

In flexion motion, the risk of allograft spacer failure was lowest for the 11 mm CO spacer (PVMS, 48.04 MPa; 44. 5%) and highest for the 14 mm CLC spacer (PVMS, 270.0 MPa; 250.2%). In extension, the risk of allograft spacer failure was highest for the 14 mm CLC spacer (PVMS: 371.40 MPa, 344.2%) and lowest for the 11 mm CO spacer (PVMS: 71.05 MPa, 65.8%). In axial rotation, the risk of

allograft spacer failure was highest for the 11 mm CC spacer (PVMS: 317.20 MPa, 294.0%) and lowest for the 14 mm CLC spacer (PVMS: 128.30 MPa, 118.9%). In lateral bending, the risk of allograft spacer failure was highest for 14 mm CLC spacers (PVMS: 244.20 MPa, 226.3%) and lowest for 14 mm CO spacers (PVMS: 150.20 MPa, 139.2%) (Figure 4).

3.3. Stress Analysis of Endplates of Involved Lower Cervical Segments

In flexion, von Mises stress increased as the lengths of spacers increased, especially at the endplates around the posterior wall of the allograft spacers, and was most prominent in the CLC spacers. In extension, von Mises stress increased as the lengths of spacers increased, especially around the posterior margin of each spacer. In both counterclockwise axial rotation and right lateral bending, von Mises stress decreased as the lengths of the spacers increased. In lateral bending, von Mises stress was higher with CLC spacers than with other spacers. The likelihood of allograft spacer subsidence was calculated on the basis of the yield strength of the cancellous bone of the C6 vertebral body (16.3 MPa). The subsidence risk was calculated using the following formula [31]:

$$\text{Subsidence risk} = \frac{Stress\ on\ the\ cortial\ portion\ of\ allograft\ spacer}{Yield\ strength\ of\ vertebral\ body(16.3\ \text{MPa})} \times 100. \tag{2}$$

In flexion motion, the risk of allograft spacer subsidence was lowest for 11 mm CO and CC spacers (PVMS, 1.41 MPa; 8.7%) and highest for the 14 mm CLC spacer (PVMS, 4.58 MPa; 28.1%). The subsidence risk was highest for the 14 mm CLC spacer (PVMS: 12.71 MPa, 78.0%) in extension, 11 mm CO and CC spacers (PVMS: 2.71 MPa, 16.6%) in axial rotation, and the 11 mm CLC spacers (PVMS 4.81 MPa, 29.5%) in lateral bending. Subsidence risk was lowest for the 11 mm CO and CC spacers (PVMS: 2.39 MPa, 14.7%) in extension, the 14 mm CO spacer (PVMS: 1.76 MPa, 10.8%) in axial rotation, and the 14 mm CO and CC spacers (PVMS: 1.13 MPa, 6.9%) in lateral bending.

4. Discussion

Graft failure with subsidence and breakage leading to non-union are major concerns in ACDF surgery and have been shown to be associated with the use an autologous bone substitute, stand-alone cages, allospacers, reinforcement with anterior plates and screws, and posterior fixation, as well as age and other factors [13,15,32–35]. However, no study has analyzed associations of biomechanical stress with cervical spacer design, length, and the ratio of cortical and cancellous portions of the spacers. It is expected that the cortical and cancellous portions play a different role once they are fused after insertion [10]. The cortical portion usually supports the endplates until the cancellous portion can form a firm union of bone. It could be postulated that a larger cortical component could result in breakage of allograft spacers or more subsidence into the vertebral body through the endplates if they fail to be fused properly postoperatively because of the different properties of E and *v* of the allograft-cortical bone and the cancellous portions of the recipient vertebral body [36]. Cortical breakage or subsidence could then result in a decrease of disc height and lead to foraminal restenosis [37]. It is commonly accepted that greater stress on the endplate and spacers and less contact with the surface of the cancellous portion could lead to an increased risk of subsidence and delayed fusion [10]. In one clinical study, CO-type allospacers, which have a smaller cancellous fusion bed, exhibited more breakage and displacement with disc height loss causing fixation instability, compared with other spacers [13]. In our study, the smaller cortical portion conversely led to an increased subsidence risk and a relatively higher risk of allograft spacer failure despite the wider fusion bed of cancellous bone, especially upon flexion and extension.

We analyzed the results of predicted FE study using von Mises stress. The reasons are as follows: Generally, stress has direction, but von Mises stress is scalar and not a vector. Therefore, it is easy to analyze stresses in various directions, such as principal stress, at complex loading on the human body. Additionally, the von Mises is a theoretical measure of stress used to estimate yield failure criteria and is also popular in fatigue strength calculations. While significant differences in von Mises stress on

different types of spacers and endplates were noted (Figure 4), the results did not fall in line with our initial hypothesis that longer spacers could supply a wider surface area of stress distribution and result in less von Mises stress on allograft spacers and endplates. The longer spacers showed a higher level of concentrated stresses on the posterior wall of the allograft spacers and in the contacted endplate area in flexion and extension. This could be explained by the nutcracker mechanism with anterior cortical-bite positioning of allograft spacers (Figure 1), wherein the longer spacer exerts greater compression force at the posterior margin of the allograft spacer and contacting endplate, as well as greater posterior shear force from the superior anterior corner to the inferior posterior corner of the allograft spacer. This could lead to allograft spacer failure or graft subsidence, even though it is known that posterior endplates are stronger than the anterior component [38]

The ROM in all motion modes was easily understandable because of the decreased ROM in the fused segment of C5–6 and increased ROM in the adjacent C4-5 and C6–7 segments. The longer spacers produced greater stress on the endplate and posterior complex of the vertebral body in flexion and extension. Along with higher preloading on the distal cervical segment, this increased stress could play a role in increased subsidence and result in a decreased ROM relative to the intact segment of C6–7. This needs to be clarified in further research.

This study had a few limitations. This study was designed only for allograft spacers and vertebral bodies without additional fixation methods, such as anterior plates and screws, lateral mass screws, or pedicle screws [15,31]. However, using our basic stress analyses on allograft spacers and endplate-vertebral bodies for spacer composition and length, a series of biomechanical studies will be performed with variable fixation methods, spacer sizes, and cervical sagittal alignments. Also, the ROM of the intact model was compared with that previously reported by Ivancic and Panjabi et al [29,30]. This approach confirmed that the kinematics of the developed FEM reflect real soft tissue functions. However, in our study, we calculated the distribution of stress on endplates, which is a different context for the use of this FEM. Therefore, this study could lack sufficient evidence in support of the validation of this FEM. Nevertheless, in many biomechanical studies, ROM was utilized to validate and verify models, as well as to predict stress and forces reflective of real-world settings [39–46]. Considering the relative comparisons between the design and lengths of the allograft spacers, the results in the present study could be helpful to understanding the biomechanical differences between allospacers.

This study could help to decide the best combination of surgical approach and type of allograft spacer depending on a patient's conditions. As a potential ethnic anthropometric limitation, the FEM model was designed for the average Korean, middle-aged male, and Caucasian individuals tend to have larger profiles than Koreans [47,48]. Additional analysis on post-menopausal women with weaker bone quality is ongoing and will provide a better understanding of biomechanical properties in that clinical settings.

5. Conclusions

Smaller cortical portions and longer cervical spacers could be risk factors for allograft spacer failure and subsidence, especially in flexion and extension, in an allograft spacer only model. However, further study in combination with additional fixation methods, such as anterior plates/screws and posterior screws, in an actual clinical setting is necessary.

References

1. Lee, C.-H.; Chung, C.-K.; Kim, C.H.; Kwon, J.-W. Health Care Burden of Spinal Diseases in the Republic of Korea: Analysis of a Nationwide Database From 2012 Through 2016. *Neurospine* **2018**, *15*, 66–76. [CrossRef] [PubMed]
2. Kotkansalo, A.; Leinonen, V.; Korajoki, M.; Salmenkivi, J.; Korhonen, K.; Malmivaara, A. Surgery for degenerative cervical spine disease in Finland, 1999–2015. *Acta Neurochir.* **2019**, *161*, 2147–2159. [CrossRef] [PubMed]
3. Yang, J.J.; Yu, C.H.; Chang, B.-S.; Yeom, J.S.; Lee, J.H.; Lee, C.-K. Subsidence and Nonunion after Anterior Cervical Interbody Fusion Using a Stand-Alone Polyetheretherketone (PEEK) Cage. *Clin. Orthop. Surg.* **2011**, *3*, 16–23. [CrossRef] [PubMed]
4. Pandita, N.; Gupta, S.; Raina, P.; Srivastava, A.; Hakak, A.Y.; Singh, O.; Darokhan, M.A.-U.-D.; Butt, M.F. Neurological Recovery Pattern in Cervical Spondylotic Myelopathy after Anterior Surgery: A Prospective Study with Literature Review. *Asian Spine J.* **2019**, *13*, 423–431. [CrossRef]
5. Viswanathan, V.K.; Manoharan, S.R. To Plate or Not to Plate after a Single- or Two-Level Anterior Cervical Discectomy: Fusion with Cage-Plate Construct or Stand-Alone Cage. *Asian Spine J.* **2017**, *11*, 1–3. [CrossRef]
6. Schmieder, K.; Wolzik-Grossmann, M.; Pechlivanis, I.; Engelhardt, M.; Scholz, M.; Harders, A. Subsidence of the Wing titanium cage after anterior cervical interbody fusion: 2-year follow-up study. *J. Neurosurg. Spine* **2006**, *4*, 447–453. [CrossRef]
7. Čabraja, M.; Oezdemir, S.; Koeppen, D.; Kroppenstedt, S. Anterior cervical discectomy and fusion: Comparison of titanium and polyetheretherketone cages. *BMC Musculoskelet. Disord.* **2012**, *13*, 172. [CrossRef]
8. Chen, Y.; Wang, X.; Lu, X.; Yang, L.; Yang, H.; Yuan, W.; Chen, D. Comparison of titanium and polyetheretherketone (PEEK) cages in the surgical treatment of multilevel cervical spondylotic myelopathy: A prospective, randomized, control study with over 7-year follow-up. *Eur. Spine J.* **2013**, *22*, 1539–1546. [CrossRef]
9. Chau, A.M.T.; Mobbs, R.J. Bone graft substitutes in anterior cervical discectomy and fusion. *Eur. Spine J.* **2009**, *18*, 449–464. [CrossRef]
10. Ryu, S.I.; Lim, J.T.; Kim, S.M.; Paterno, J.; Willenberg, R.; Kim, D.H. Comparison of the biomechanical stability of dense cancellous allograft with tricortical iliac autograft and fibular allograft for cervical interbody fusion. *Eur. Spine J.* **2006**, *15*, 1339–1345. [CrossRef]
11. Lee, J.C.; Jang, H.-D.; Ahn, J.; Choi, S.-W.; Kang, D.; Shin, B.-J. Comparison of Cortical Ring Allograft and Plate Fixation with Autologous Iliac Bone Graft for Anterior Cervical Discectomy and Fusion. *Asian Spine J.* **2019**, *13*, 258–264. [CrossRef] [PubMed]
12. Ordway, N.R.; Rim, B.C.; Tan, R.; Hickman, R.; Fayyazi, A.H. Anterior cervical interbody constructs: Effect of a repetitive compressive force on the endplate. *J. Orthop. Res.* **2011**, *30*, 587–592. [CrossRef] [PubMed]
13. Park, K.J.; Kim, D.H.; Park, K.D.; Park, J.H.; Yoo, N.K.; Cho, K.H.; Kim, S.H. Clinical Outcomes and Finite Element Method Results of Anterior Cervical Discectomy and Fusion Using H-Beam Shaped Allospacer: A Comparison with Rim-Shaped Allospacer. *Nerve* **2019**, *5*, 49–54. [CrossRef]
14. Jung, T.-G.; Woo, S.-H.; Park, K.-M.; Jang, J.-W.; Han, D.-W.; Lee, S.J. Biomechanical behavior of two different cervical total disc replacement designs in relation of concavity of articular surfaces: ProDisc-C® vs. Prestige-LP®. *Int. J. Precis. Eng. Manuf.* **2013**, *14*, 819–824. [CrossRef]
15. Kwon, J.-W.; Bang, S.H.; Park, T.H.; Lee, S.-J.; Lee, H.-M.; Lee, S.-B.; Lee, B.H.; Moon, S.-H. Biomechanical comparison of cervical discectomy/fusion model using allograft spacers between anterior and posterior fixation methods (lateral mass and pedicle screw). *Clin. Biomech.* **2020**, *73*, 226–233. [CrossRef]
16. Galbusera, F.; Bellini, C.M.; Raimondi, M.T.; Fornari, M.; Assietti, R. Cervical spine biomechanics following implantation of a disc prosthesis. *Med. Eng. Phys.* **2008**, *30*, 1127–1133. [CrossRef]
17. Ritzel, H.; Amling, M.; Pösl, M.; Hahn, M.; Delling, G. The Thickness of Human Vertebral Cortical Bone and its Changes in Aging and Osteoporosis: A Histomorphometric Analysis of the Complete Spinal Column from Thirty-Seven Autopsy Specimens. *J. Bone Miner. Res.* **1997**, *12*, 89–95. [CrossRef]
18. Zhang, Q.H.; Teo, E.C.; Ng, H.W.; Lee, V.S.; Lee, P.V.S. Finite element analysis of moment-rotation relationships for human cervical spine. *J. Biomech.* **2006**, *39*, 189–193. [CrossRef]

19. Ha, S.K. Finite element modeling of multi-level cervical spinal segments (C3–C6) and biomechanical analysis of an elastomer-type prosthetic disc. *Med. Eng. Phys.* **2006**, *28*, 534–541. [CrossRef]

20. Kim, J.-D.; Kim, N.-S.; Hong, C.-S.; Oh, C.-Y. Design optimization of a xenogeneic bone plate and screws using the Taguchi and finite element methods. *Int. J. Precis. Eng. Manuf.* **2011**, *12*, 1119–1124. [CrossRef]

21. Whyne, C.M.; Hu, S.S.; Klisch, S.; Lotz, J.C. Effect of the Pedicle and Posterior Arch on Vertebral Body Strength Predictions in Finite Element Modeling. *Spine* **1998**, *23*, 899–907. [CrossRef] [PubMed]

22. Faizan, A.; Goel, V.K.; Garfin, S.R.; Bono, C.M.; Serhan, H.; Biyani, A.; Elgafy, H.; Krishna, M.; Friesem, T. Do design variations in the artificial disc influence cervical spine biomechanics? A finite element investigation. *Eur. Spine J.* **2009**, *21*, 653–662.

23. Harrison, D.E.; Harrison, D.D.; Cailliet, R.; Troyanovich, S.J.; Janik, T.J.; Holland, B. Cobb Method or Harrison Posterior Tangent Method: Which to choose for lateral cervical radiographic analysis. *Spine* **2000**, *25*, 2072–2078. [CrossRef] [PubMed]

24. Shi, D.; Wang, F.; Wang, N.; Li, X.; Wang, Q. 3-D finite element analysis of the influence of synovial condition in sacroiliac joint on the load transmission in human pelvic system. *Med. Eng. Phys.* **2014**, *36*, 745–753. [CrossRef]

25. Black, J.; Hastings, G. *Handbook of Biomaterial Properties*; Springer: Berlin/Heidelberg, Germany, 1998.

26. Smith, G.W.; Robinson, R.A. The Treatment of Certain Cervical-Spine Disorders by Anterior Removal of the Intervertebral Disc and Interbody Fusion. *J. Bone Jt. Surg.* **1958**, *40*, 607–624. [CrossRef]

27. Sis, H.L.; Mannen, E.M.; Wong, B.M.; Cadel, E.S.; Bouxsein, M.L.; Anderson, D.E.; Friis, E.A. Effect of follower load on motion and stiffness of the human thoracic spine with intact rib cage. *J. Biomech.* **2016**, *49*, 3252–3259. [CrossRef]

28. Panjabi, M.M. Hybrid multidirectional test method to evaluate spinal adjacent-level effects. *Clin. Biomech.* **2007**, *22*, 257–265. [CrossRef]

29. Panjabi, M.M.; Crisco, J.J.; Vasavada, A.; Oda, T.; Cholewicki, J.; Nibu, K.; Shin, E. Mechanical Properties of the Human Cervical Spine as Shown by Three-Dimensional Load–Displacement Curves. *Spine* **2001**, *26*, 2692–2700. [CrossRef]

30. Ivancic, P.C. Biomechanics of Sports-Induced Axial-Compression Injuries of the Neck. *J. Athl. Train.* **2012**, *47*, 489–497. [CrossRef]

31. Kwon, J.-W.; Bang, S.-H.; Kwon, Y.-W.; Cho, J.-Y.; Park, T.-H.; Lee, S.-J.; Lee, H.-M.; Moon, S.-H.; Lee, B.-H. Biomechanical comparison of the angle of inserted screws and the length of anterior cervical plate systems with allograft spacers. *Clin. Biomech.* **2020**, *76*, 105021. [CrossRef]

32. Kao, T.H.; Wu, C.H.; Chou, Y.C.; Chen, H.T.; Chen, W.H.; Tsou, H.K. Risk factors for subsidence in anterior cervical fusion with stand-alone polyetheretherketone (PEEK) cages: A review of 82 cases and 182 levels. *Arch. Orthop. Trauma Surg.* **2014**, *134*, 1343–1351. [CrossRef] [PubMed]

33. Goel, V.K.; Faizan, A.; Palepu, V.; Bhattacharya, S. Parameters that effect spine biomechanics following cervical disc replacement. *Eur. Spine J.* **2012**, *21*, 688–699. [CrossRef] [PubMed]

34. Lee, Y.S.; Kim, Y.B.; Park, S.W. Risk factors for postoperative subsidence of single-level anterior cervical discectomy and fusion: The significance of the preoperative cervical alignment. *Spine (Phila Pa 1976)* **2014**, *39*, 1280–1287. [CrossRef] [PubMed]

35. De Leo–Vargas, R.A.; Muñoz–Romero, I.; Mondragón–Soto, M.G.; Martínez–Anda, J.J. Locking Stand-Alone Cage Constructs for the Treatment of Cervical Spine Degenerative Disease. *Asian Spine J.* **2019**, *13*, 630. [CrossRef]

36. Roberts, T.T.; Rosenbaum, A.J. Bone grafts, bone substitutes and orthobiologics: The bridge between basic science and clinical advancements in fracture healing. *Organogenesis* **2012**, *8*, 114–124. [CrossRef]

37. Karikari, I.O.; Jain, D.; Owens, T.R.; Gottfried, O.; Hodges, T.R.; Nimjee, S.M.; Bagley, C.A. Impact of subsidence on clinical outcomes and radiographic fusion rates in anterior cervical discectomy and fusion: A systematic review. *J. Spinal Disord. Tech.* **2014**, *27*, 1–10. [CrossRef]

38. Cheng, C.C.; Ordway, N.R.; Zhang, X.; Lu, Y.M.; Fang, H.; Fayyazi, A.H. Loss of cervical endplate integrity following minimal surface preparation. *Spine (Phila Pa 1976)* **2007**, *32*, 1852–1855. [CrossRef]

39. Chiang, M.-F.; Teng, J.-M.; Huang, C.-H.; Cheng, C.-K.; Chen, C.-S.; Chang, T.-K.; Chao, S.-H. Finite element analysis of cage subsidence in cervicalinterbody fusion. *J. Med. Biol. Eng.* **2004**, *24*, 201–208.

40. Liu, N.; Lu, T.; Wang, Y.; Sun, Z.; Li, J.; He, X. Effects of new cage profiles on the improvement in biomechanical performance of multilevel anterior cervical Corpectomy and fusion: A finite element analysis. *World Neurosurg.* **2019**, *129*, e87–e96. [CrossRef]

41. Zhang, Y.; Zhou, J.; Guo, X.; Cai, Z.; Liu, H.; Xue, Y. Biomechanical Effect of Different Graft Heights on Adjacent Segment and Graft Segment Following C4/C5 Anterior Cervical Discectomy and Fusion: A Finite Element Analysis. *Med. Sci. Monit. Int. Med J. Exp. Clin. Res.* **2019**, *25*, 4169. [CrossRef]

42. Wang, J.; Qian, Z.; Ren, L. Biomechanical Comparison of Optimal Shapes for the Cervical Intervertebral Fusion Cage for C5–C6 Cervical Fusion Using the Anterior Cervical Plate and Cage (ACPC) Fixation System: A Finite Element Analysis. *Med. Sci. Monit. Int. Med. J. Exp. Clin. Res.* **2019**, *25*, 8379. [CrossRef]

43. Lee, J.H.; Park, W.M.; Kim, Y.H.; Jahng, T.-A. A biomechanical analysis of an artificial disc with a shock-absorbing core property by using whole-cervical spine finite element analysis. *Spine* **2016**, *41*, E893–E901. [CrossRef]

44. Lee, S.-H.; Im, Y.-J.; Kim, K.-T.; Kim, Y.-H.; Park, W.-M.; Kim, K. Comparison of cervical spine biomechanics after fixed-and mobile-core artificial disc replacement: A finite element analysis. *Spine* **2011**, *36*, 700–708. [CrossRef] [PubMed]

45. Lin, C.-Y.; Chuang, S.-Y.; Chiang, C.-J.; Tsuang, Y.-H.; Chen, W.-P. Finite element analysis of cervical spine with different constrained types of total disc replacement. *J. Mech. Med. Biol.* **2014**, *14*, 1450038. [CrossRef]

46. Kim, Y.H.; Khuyagbaatar, B.; Kim, K. Recent advances in finite element modeling of the human cervical spine. *J. Mech. Sci. Technol.* **2018**, *32*, 1–10. [CrossRef]

47. Kim, M.K.; Kwak, D.S.; Park, C.K.; Park, S.H.; Oh, S.M.; Lee, S.W.; Han, S.H. Quantitative anatomy of the endplate of the middle and lower cervical vertebrae in Koreans. *Spine (Phila Pa 1976)* **2007**, *32*, E376–E381. [CrossRef] [PubMed]

48. Yao, Q.; Yin, P.; Khan, K.; Tsai, T.Y.; Li, J.S.; Hai, Y.; Tang, P.; Li, G. Differences of the Morphology of Subaxial Cervical Spine Endplates between Chinese and White Men and Women. *Biomed. Res. Int.* **2018**, *2018*, 2854175. [CrossRef] [PubMed]